SEMI-BLIND SEPARATION OF GALAXY SPECTRA FROM A MIXTURE OBTAINED BY SLITLESS SPECTROSCOPY

Ahmed Selloum, Shahram Hosseini, Thierry Contini, Yannick Deville

IRAP, CNRS, Université de Toulouse, UPS-OMP. 14, av. Edouard Belin, 31400 Toulouse, France.
{ ahmed.selloum, shahram.hosseini, thierry.contini, yannick.deville } @irap.omp.eu

ABSTRACT

We investigate the problem of separating galaxy spectra from their mixtures resulting from the slitless spectroscopy used in the future Euclid space mission. This can be formulated as a source separation problem where the structure of the mixture is specific and depends on a low number of parameters. We first develop a mathematical model to describe the observations generated by the near-infrared spectrograph of Euclid, then propose non-blind, semi-blind and regularized semi-blind methods to separate the spectra. The first simulation results are encouraging: even for a signal to noise ratio of 5 dB, our regularized semi-blind method succeeds in separating the considered two spectra and provides a satisfactory estimate of the emission line positions and amplitudes.

Index Terms— Semi-blind source separation, Euclid mission, Spectrum decontamination, Slitless spectroscopy, Optimization

1. INTRODUCTION

Euclid is an astronomy space mission under development by the European Space Agency (ESA) [1]. Its launch is currently planned for 2020. Its main mission is to better understand the nature of dark energy, which represents around 68 % of the Universe [2], and is generally accepted to be the source of the increased acceleration of the Universe expansion. To this end, Euclid will survey the sky with a near-infrared slitless spectrograph providing spectra of about 50 million galaxies. These spectra will be analyzed to measure the galaxy redshifts, i.e. increases in wavelength of emission lines due to the expansion of the Universe. This measurement is based on the detection of emission lines, mainly $H\alpha$, in the spectra[1].

The near-infrared spectrograph of Euclid will be equipped with low-resolution grisms. A grism is a combination of a diffraction grating and a prism, and is used to generate a dispersed spectrum (called a 2D spectrum) of astronomical objects. In general, spectroscopy in astronomy is performed with a slit, allowing light from only a limited region of the sky (e.g. a star or a galactic nucleus) to be diffracted. Slitless spectroscopy, used in Euclid, is however affected by the confusion resulting from the superposition of 2D spectra of neighboring objects. As an example, Figure 1 shows a special case when the dispersed 2D spectra of two objects are mixed. As mentioned in [3], *at the depth of Euclid spectroscopic observations, essentially every spectrum is at least partially superimposed to another. In such conditions, this contamination is the main cause of redshift measurement failures,* so that *reducing confusion produced by overlapping spectra is the first concern.*

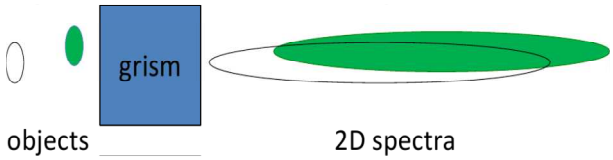

Fig. 1. Contamination of neighboring object spectra.

The decontamination of Eulid spectra may be considered as a source separation problem which consists in estimating a set of unknown source signals from their observed mixtures. In the usual *blind* case, one aims at estimating both the source signals and the mixing model parameters. Blind source separation algorithms are mainly based on statistical independence of source signals, their non-negativity, or their sparseness [4]. Nevertheless, when the mixing model is totally or partially known, non-blind or semi-blind approaches may also be used [5, 6]. In the following, we first propose a mathematical model describing the observed data obtained with slitless spectrographs, then use this model to develop non-blind and semi-blind source separation methods. In this paper, we only consider first-order spectra generated by one grism in one direction.

2. OBSERVATION MODELING

2.1. Signal model before the telescope

The signal before being observed by the telescope is composed of astronomical objects (mainly galaxies) and the sky

This work has been partially funded by CNES (Centre National d'Etudes Spatiales, France).

[1] $H\alpha$ is the brightest emission line observed in the spectrum of star-forming galaxies, which occurs when a hydrogen electron falls from its third to its second orbit.

978-0-9928626-3-3/15/$31.00 ©2015 IEEE

background. In the following, we assume that a precise estimate of the sky background is available so that its contribution can be subtracted from the observations. Thus, we do not consider it below. Each object with index i may be defined by its spectrum, $s_i(\lambda)$, its center position, $z_i = [x_i, y_i]$, and the parameters describing its light profile (and as a result its shape). Hereafter, we assume that:

H1: The normalized spectrum for each object (i.e. its spectral energy distribution) is the same for all object points.

H2: The light profile, i.e. the intensity of light in each point of an object (as a function of its position with respect to the object center) can be modeled by a 2D Gaussian function.

The three parameters of this Gaussian function (σ_{a_i}, σ_{b_i}, r_i) can be determined from the object shape by modeling this shape by an ellipse, characterized by its major axis, its minor axis and its rotation angle.

H1 is realistic for most of galaxies. H2 may be replaced by more precise models of the light profile but can be used as an approximation of the real model: it has been used in the Euclid near-infrared spectrograph simulator (called TIPS) [7].

According to H1, the light intensity of an object with index i, at a wavelength λ and at a point with coordinates (x, y) can be modeled as $q_i(x, y, \lambda) = s_i(\lambda) f_i(x - x_i, y - y_i)$, where ($x_i$, y_i) corresponds to the object center position and $f_i(x - x_i, y - y_i)$ represents its light profile. Thanks to H2, this light profile reads

$$f_i(x - x_i, y - y_i) = \mathcal{N}\left(\begin{bmatrix} x_i \\ y_i \end{bmatrix}, \begin{bmatrix} \sigma_{a_i}^2 & r_i\sigma_{a_i}\sigma_{b_i} \\ r_i\sigma_{a_i}\sigma_{b_i} & \sigma_{b_i}^2 \end{bmatrix}\right) \quad (1)$$

where $\mathcal{N}(\boldsymbol{\mu}, \boldsymbol{\Sigma})$ represents a 2D Gaussian function with mean $\boldsymbol{\mu}$ and covariance $\boldsymbol{\Sigma}$.

2.2. Object model after the PSF and before the grism

We assume that:

H3: The PSF (Point Spread Function) of the instrument can be modeled by a linear combination of two circular 2D Gaussian functions. This model is defined by three parameters (σ_1, σ_2, c = weighting coefficient):

$$h(x, y) = c\mathcal{N}\left(\begin{bmatrix} 0 \\ 0 \end{bmatrix}, \begin{bmatrix} \sigma_1^2 & 0 \\ 0 & \sigma_1^2 \end{bmatrix}\right) + (1 - c)\mathcal{N}\left(\begin{bmatrix} 0 \\ 0 \end{bmatrix}, \begin{bmatrix} \sigma_2^2 & 0 \\ 0 & \sigma_2^2 \end{bmatrix}\right). \quad (2)$$

This model has been admitted to be sufficiently flexible for providing a good approximation of the instrument PSF [8], and has been used in the TIPS simulator [7]. In the general case, the parameters of this model may change with wavelength and position. However, in the current paper, we do not take these variations into account. Anyway, the PSF variations being slow, it can be considered as locally constant.

Each object with index i is spatially spread because of its convolution with the instrument PSF. Thus, one obtains a "new object" whose light intensity is defined by the following equation:

$$\begin{aligned} w_i(x, y, \lambda) &= \int\int_{\mathbb{R}^2} q_i(u, v, \lambda) h(x - u, y - v) du dv \\ &= s_i(\lambda)[f_i(x - x_i, y - y_i) * h(x, y)] \\ &= s_i(\lambda) I_i(x - x_i, y - y_i), \end{aligned} \quad (3)$$

where I_i represents "f_i convolved by h".

The convolution of two Gaussian functions is a Gaussian function whose mean and covariance matrix are respectively the sum of means and the sum of covariance matrices of the two original Gaussian functions. Consequently:

$$\begin{aligned} &I_i(x - x_i, y - y_i) = \\ &c\mathcal{N}\left(\begin{bmatrix} x_i \\ y_i \end{bmatrix}, \begin{bmatrix} \sigma_{a_i}^2 + \sigma_1^2 & r_i\sigma_{a_i}\sigma_{b_i} \\ r_i\sigma_{a_i}\sigma_{b_i} & \sigma_{b_i}^2 + \sigma_1^2 \end{bmatrix}\right) \\ &+(1 - c)\mathcal{N}\left(\begin{bmatrix} x_i \\ y_i \end{bmatrix}, \begin{bmatrix} \sigma_{a_i}^2 + \sigma_2^2 & r_i\sigma_{a_i}\sigma_{b_i} \\ r_i\sigma_{a_i}\sigma_{b_i} & \sigma_{b_i}^2 + \sigma_2^2 \end{bmatrix}\right). \end{aligned} \quad (4)$$

2.3. Object model after the grism

The observed image is then dispersed by a grism which may generate spectra of different orders [9]. The grism will be optimized to concentrate most of light energy in the first-order spectrum. However, zero-order and second-order spectra may be non-negligible, specially for very bright objects. In this paper, only the first-order spectrum will be considered. Nevertheless, the consideration of the other orders does not fundamentally change the approach proposed in our paper.

The extension of the spectrum in the focal plane of detectors is called the *trace*, which may be curved [9]. In this paper, we assume that its curvature is negligible so that the trace will be modeled by a horizontal line. The *dispersion* defines the wavelength-domain resolution of the dispersed light. Considering a horizontal trace (in the x direction), for an object with index i, we obtain at the grism output a 2D dispersed image which reads [10]:

$$t_i(x, y) = \int_{\Omega_\lambda} w_i\left(x - D(\lambda), y, \lambda\right) d\lambda, \quad (5)$$

where Ω_λ is the wavelength range covered by the grism and $D(\lambda)$ represents the dispersion function in the x direction. Using (3), and assuming a linear dispersion $D(\lambda) = a\lambda + b$, we obtain

$$t_i(x, y) = \int_{\Omega_\lambda} I_i(x - x_i - a\lambda - b, y - y_i) s_i(\lambda) d\lambda. \quad (6)$$

The above equation is established for real (i.e. non-integer) values of x and y. In practice, the measured signal in a pixel of detector, for an object with index i, is the integral of $t_i(x, y)$

over the surface Ω_p of that pixel. The measured value for a pixel with index p is then:

$$o_i(p) = \int\int_{(x,y)\in\Omega_p} t_i(x,y)dxdy. \quad (7)$$

Substituting $t_i(x,y)$ by its definition and after the discretization of the integrals using the rectangle method, we finally obtain

$$o_i(p) = \sum_{l/\lambda_l\in\Omega_\lambda} m_i(p,\lambda_l)s_i(\lambda_l), \quad (8)$$

with

$$m_i(p,\lambda_l) = \sum_{j,k/(x_j,y_k)\in\Omega_p}\sum I_i(x_j - x_i - a\lambda_l - b, y_k - y_i)\Delta x\Delta y\Delta\lambda, \quad (9)$$

where the step sizes Δx, Δy, $\Delta\lambda$ must be chosen according to the resolution of the instrument and in particular the detectors.

2.4. Mixing model

When a pixel with index p receives photons from N objects, the measured value in that pixel reads

$$o(p) = \sum_{i=1}^{N} o_i(p) = \sum_{i=1}^{N}\sum_{l=1}^{L} m_i(p,\lambda_l)s_i(\lambda_l), \quad (10)$$

where L is the number of considered wavelengths. Considering measured values in P pixels which receive radiations from N objects, we can then collect all these measured values in a vector $\mathbf{o} = [o(1), ..., o(P)]^T$. The mixing equation can then be written in the following matrix form:

$$\mathbf{o} = \mathbf{M}\mathbf{s}, \quad (11)$$

where $\mathbf{s} = [\mathbf{s}_1^T, \mathbf{s}_2^T, ..., \mathbf{s}_N^T]^T$ represents the global vector of sources with $\mathbf{s}_i = [s_i(\lambda_1), s_i(\lambda_2), ..., s_i(\lambda_L)]^T$. The mixing matrix $\mathbf{M}$ is the result of the concatenation of N matrices $\mathbf{M}_i$:

$$\mathbf{M} = [\mathbf{M}_1, \mathbf{M}_2, \cdots, \mathbf{M}_N], \quad (12)$$

where the entry (p,l) of each matrix $\mathbf{M}_i$ (of size $P \times L$) is equal to $m_i(p,\lambda_l)$ defined in (9). The mixture is overdetermined if $P > (L \times N)$.

The mathematical model proposed in this section is the basis for the development of our source separation algorithms, presented in the following section.

3. SOURCE SEPARATION METHODS

3.1. Non-blind method

In this first method, it is assumed that the object positions $z_i = [x_i, y_i]$, the parameters of the shape of each object $(\sigma_{a_i}, \sigma_{b_i}, r_i)$, and the PSF parameters (σ_1, σ_2, c) are known. From these parameters, and subject to the validity of the model described in the previous section, we can first calculate the mixing matrix $\mathbf{M}$, then use the mixing model to obtain a least squares estimate of the sources by minimizing the criterion $J_1 = ||\mathbf{o} - \mathbf{M}\mathbf{s}||_2^2$:

$$\hat{\mathbf{s}} = (\mathbf{M}^T\mathbf{M})^{-1}\mathbf{M}^T\mathbf{o}. \quad (13)$$

3.2. Semi-blind method

In practice, the model proposed in the previous section would not perfectly match the instrument model and its parameters are not perfectly known. As a result, the non-blind method is unlikely to provide satisfactory results. Thus, we propose a more flexible semi-blind method which estimates the parameters of the PSF, as well as the shape parameters of each object together with the object spectra. Consider the vector of unknown parameters $\boldsymbol{\theta} = [\sigma_1, \sigma_2, c, \{\sigma_{a_i}, \sigma_{b_i}, r_i\}_{i\in\{1,...,N\}}]^T$ and suppose that $\boldsymbol{\theta} \in [\boldsymbol{\theta}_{min}, \boldsymbol{\theta}_{max}]$. In this method, we assume that $\boldsymbol{\theta}$ is unknown but its variation domain, defined by the extreme values $\boldsymbol{\theta}_{min}$ and $\boldsymbol{\theta}_{max}$, is known (using the physical constraints, the direct images, and our knowledge on the instrument characteristics). We also assume that the object center positions are known, thanks to the direct images.

The idea here is to minimize $J_2 = ||\mathbf{o} - \mathbf{M}(\boldsymbol{\theta})\mathbf{s}||_2^2$ with respect to both $\boldsymbol{\theta}$ and $\mathbf{s}$ under the constraint $\boldsymbol{\theta} \in [\boldsymbol{\theta}_{min}, \boldsymbol{\theta}_{max}]$. A simple and fast solution is to consider the optimal value of $\mathbf{s}$ that minimizes the criterion J_2 for a given value of $\boldsymbol{\theta}$, i.e. $\hat{\mathbf{s}} = [\mathbf{M}(\boldsymbol{\theta})^T\mathbf{M}(\boldsymbol{\theta})]^{-1}\mathbf{M}(\boldsymbol{\theta})^T\mathbf{o}$, to insert this value in the criterion J_2 which yields:

$$J_2(\boldsymbol{\theta}) = ||\mathbf{o} - \mathbf{M}(\boldsymbol{\theta})[\mathbf{M}(\boldsymbol{\theta})^T\mathbf{M}(\boldsymbol{\theta})]^{-1}\mathbf{M}(\boldsymbol{\theta})^T\mathbf{o}||_2^2, \quad (14)$$

and to run the following two-step algorithm:

1. Estimation of $\boldsymbol{\theta}$**:**
   we use the `fmincon` MATLAB® function to solve the following constrained optimization problem:
   $$\widehat{\boldsymbol{\theta}} = min\left(J_2(\boldsymbol{\theta})|\boldsymbol{\theta} \in [\boldsymbol{\theta}_{min}, \boldsymbol{\theta}_{max}]\right). \quad (15)$$
2. Estimation of $\mathbf{s}$**:**
   we calculate the mixing matrix $\mathbf{M}(\widehat{\boldsymbol{\theta}})$ from $\widehat{\boldsymbol{\theta}}$ estimated in the first step, and we deduce from it the estimator of spectra: $\hat{\mathbf{s}} = [\mathbf{M}(\widehat{\boldsymbol{\theta}})^T\mathbf{M}(\widehat{\boldsymbol{\theta}})]^{-1}\mathbf{M}(\widehat{\boldsymbol{\theta}})^T\mathbf{o}$.

3.3. Regularized method

In a least squares problem, the matrix $\mathbf{M}$ can be ill-conditioned, leading to a large number of possible solutions. In this case, the addition of a regularization term can generally improve results. Tikhonov regularization aims to improve the conditioning of the problem by favoring a particular solution with properties that seem relevant. The regularized criterion then reads $J_3 = ||\mathbf{o} - \mathbf{M}\mathbf{s}||_2^2 + ||\boldsymbol{\Gamma}\mathbf{s}||_2^2$ where $\boldsymbol{\Gamma}$, the Tikhonov

matrix, should be selected for the particular problem. In our problem, we chose the following difference matrix to impose a smoothing constraint:

$$\mathbf{\Gamma} = \alpha \begin{bmatrix} 2 & -1 & 0 & \cdots & 0 \\ -1 & 2 & -1 & \ddots & \ddots \\ 0 & -1 & 2 & -1 & \ddots \\ \ddots & \ddots & \ddots & \ddots & \ddots \\ 0 & \cdots & 0 & -1 & 2 \end{bmatrix}, \quad (16)$$

where the parameter α allows us to choose the weight of the regularization term in the overall criterion. If the mixing matrix $\mathbf{M}(\boldsymbol{\theta})$ is known, the minimum of J_3 is achieved for

$$\hat{\mathbf{s}} = (\mathbf{M}(\boldsymbol{\theta})^T\mathbf{M}(\boldsymbol{\theta}) + \mathbf{\Gamma}^T\mathbf{\Gamma})^{-1}\mathbf{M}(\boldsymbol{\theta})^T\mathbf{o}. \quad (17)$$

Otherwise, we use the same approach as in Section 3.2, i.e. we insert the above expression of $\hat{\mathbf{s}}$ in J_3 which yields:

$$J_3(\boldsymbol{\theta}) = ||\mathbf{o} - \mathbf{M}(\boldsymbol{\theta})[\mathbf{M}(\boldsymbol{\theta})^T\mathbf{M}(\boldsymbol{\theta}) + \mathbf{\Gamma}^T\mathbf{\Gamma}]^{-1}\mathbf{M}(\boldsymbol{\theta})^T\mathbf{o}||_2^2 + ||\mathbf{\Gamma}[\mathbf{M}(\boldsymbol{\theta})^T\mathbf{M}(\boldsymbol{\theta}) + \mathbf{\Gamma}^T\mathbf{\Gamma}]^{-1}\mathbf{M}(\boldsymbol{\theta})^T\mathbf{o}||_2^2, \quad (18)$$

then, we estimate $\hat{\boldsymbol{\theta}}$ by the constrained minimization of (18), and we deduce $\hat{\mathbf{s}}$ from it using (17).

4. SIMULATION RESULTS

4.1. Simulated data

The TIPS simulator [7] was used to simulate the observed images of Euclid from a source catalog containing their locations, magnitudes, shapes, and spectra. We chose a simple simulation scenario using two realistic sources (galaxies with redshifts 1.24 and 1.7). According to the simulator documentation, the chosen parameters to simulate the PSF are $\sigma_1 = 0.5$, $\sigma_2 = 2.8$, and $c = 0.75$. The two objects are placed very close in the scene so that their spectra are highly overlapping. The 2D spectrum corresponding to the 0 degree red grism, obtained at the output of the simulator and shown in Figure 2.a, is a mixture of the two original spectra. Knowing the positions of the objects, we chose five rows of pixels (corresponding to $x \in [862, 1506]$ and $y \in [958, 962]$ in Figure 2.a) to build the observation vector $\mathbf{o}$. Figure 2.b shows the elements of this vector.

4.2. Results using noiseless data

After applying the non-blind method (using the same parameters as those used in the simulator), we observed that the estimated spectra did not exactly match the actual spectra. This estimation error is due to the mismatch between our observation model developed in Section 2 and the model used in the TIPS simulator. For example, the spatial and spectral step sizes used in our observation model do not exactly correspond

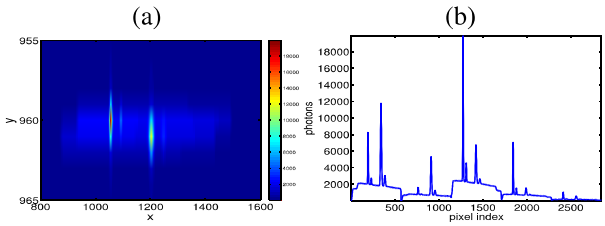

Fig. 2. (a) The 2D spectrum obtained at the TIPS output. (b) The observation vector.

to those used in the TIPS simulator. These results illustrate the main drawback of non-blind methods: they are highly model-dependent. Indeed, if the model is totally correct, these methods provide a very good estimate of the sources, but any modeling error leads to unavoidable estimation errors.

We then tested our semi-blind method using the same data, which led to a nearly perfect estimation of both spectra. The Normalized Mean Square Error between the estimated and actual spectra, defined as

$$NMSE = \underset{\lambda}{mean}[(s_i(\lambda) - \hat{s}_i(\lambda))^2]/\underset{\lambda}{mean}[(s_i(\lambda))^2], \quad (19)$$

was 1.13% for object 1 and 0.82% for object 2.

4.3. Results using noisy data

We then added white Gaussian noise to the observations, to obtain a Signal to Noise Ratio (SNR) of 10 dB. The elements of the noisy observation vector are presented in Figure 3. In

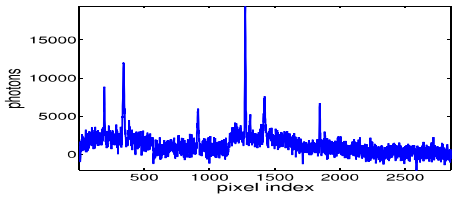

Fig. 3. Noisy observation vector.

this case, our non-regularized semi-blind method led to a poor estimation of the original spectra (see Figure 4.a).

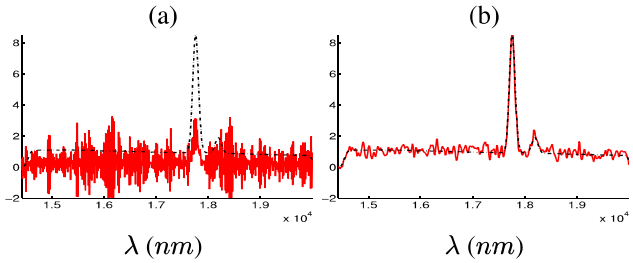

Fig. 4. Comparison between the estimated spectrum (red solid line) and the actual spectrum (black dashed line) of object 2: (a) non-regularized semi-blind method, (b) regularized semi-blind method.

Then, we applied our regularized method using different values of the weighting parameter α, which led to a much better estimation. Figure 4.b shows the results obtained with $\alpha = 5$, which confirms the effectiveness of this method.

We also repeated the experiment using stronger noise, corresponding to an SNR of 5 dB. To measure the performance of our method applied to noisy data, we can use the NMSE criterion defined in (19). However, this criterion is not easily interpretable. Indeed, our method does not aim at denoising source spectra but at separating them. Even when the two sources are perfectly separated, the NMSE criterion may have high values due to the noise present in the estimated spectra. Therefore, we propose the following additional criteria to measure the quality of estimation of the emission lines:

- Relative error on the estimation of the position of the main emission line, defined as $E_{pos} = (\lambda_{peak} - \hat{\lambda}_{peak})/\lambda_{peak}$.
- Relative error on the estimation of the amplitude of the main emission line, defined as $E_{amp} = [s_i(\lambda_{peak}) - \hat{s}_i(\hat{\lambda}_{peak})]/s_i(\lambda_{peak})$.

Table 1. Estimation errors (in %).

SNR	α	Object	$NMSE$	E_{pos}	E_{amp}
10 dB	2	1	4.18	0.06	7.28
		2	4.85	0.06	1.22
	5	1	2.70	0.06	6.69
		2	2.73	0.00	1.98
	10	1	2.26	0.06	8.62
		2	2.19	0.00	2.2
5 dB	2	1	11.51	0.06	11.58
		2	13.88	0.11	11.48
	5	1	7.46	0.00	8.64
		2	8.38	0.11	10.81
	10	1	6.12	0.00	9.94
		2	6.43	0.06	10.19

Table 1 summarizes the results, which confirm the good performance of our regularized method even in the presence of high-level noise. Not surprisingly, the method performs better when the SNR is higher. We remarked that the NMSE decreases when α increases. This can be explained by the effect of lowpass filtering, due to the smoothing constraint, which contributes to the denoising of the estimated spectra. However, if the value of α is increased too much, a deterioration in the estimation of the amplitude of the main peak is observed. In the general case, the choice of this parameter is the result of a trade-off between the smoothing constraint and the least squares criterion and generally depends on the SNR. In these tests, the choice of $\alpha = 5$ gives the best overall result.

5. CONCLUSION

In this paper, we first developed a mathematical model to describe the observations generated by the near-infrared spectrograph of Euclid, then proposed non-blind and semi-blind methods to separate the spectra of different objects. The first simulation results are encouraging. Even for an SNR of 5 dB, our regularized semi-blind method succeeds in separating the considered two spectra and provides a satisfactory estimate of the position and the amplitude of the Hα lines.

In our future works, we will perform other tests in other configurations and with more realistic assumptions (non-stationary noise, variant PSF). Moreover, so far we only considered the observations obtained with a single grism and in a single orientation angle. The exploitation of observations from all the available grisms and angles will yield better results. We must also take into account the zero-order and second-order spectra generated by the grisms and the possible curvature of the dispersed spectra.

Acknowledgment

We would like to thank J. Zoubian for helpful discussions.

REFERENCES

[1] Euclid Consortium page, http://www.euclid-ec.org/

[2] NASA Science: astrophysics, http://science.nasa.gov /astrophysics/focus-areas/what-is-dark-energy

[3] Euclid Definition Study Report (Redbook), http://arxiv.org/ftp/arxiv/papers/1110/1110.3193.pdf, ESA, 2011.

[4] P. Comon and C. Jutten Eds., *Handbook of blind source separation. Independent component analysis and applications*. Academic Press, Oxford, 2010.

[5] A. Selloum, Y. Deville, H. Carfantan, Separation of stellar spectra from hyperspectral images using particle filtering constrained by a parametric spatial mixing model, in *Proc. of ECMSM'2013*, June 2013, Toulouse, France.

[6] I. Meganem, S. Hosseini, Y. Deville, Positivity-based separation of stellar spectra using a parametric mixing model, in *Proc. of Eusipco'2013*, Sept. 2013, Marrakech, Morocco.

[7] TIPS Simulator page, http://projects.lam.fr/projects/tips/

[8] J. Zoubian, *Observations cosmologiques avec un télescope grand champ spatial : Simulations pixels du spectromètre sans fente d'EUCLID*, PhD thesis (in French), May 2012.

[9] M. Kümmel, J. R. Walsh, N. Pirzkal, H. Kuntschner, A. Pasquali, The Slitless Spectroscopy Data Extraction Software, *Publications of the Astronomical Society of the Pacific (PASP)*, 121:59-72, Jan. 2009.

[10] W. Freudling et al., The Hubble Legacy Archive NICMOS grism data, *A&A* 490, 1165-1179, 2008.